Imaging Multiple MicroRNAs in Living Cell by ATP Self-Powered Strand-Displacement Cascade Amplification

Xiangdan Meng, Wenhao Dai, Kai Zhang, Haifeng Dong,* and Xueji Zhang*

Research Center for Bioengineering and Sensing Technology, University of Science & Technology Beijing

30 Xueyuan Road, Beijing 100083, P. R. China

E-mail: zhangxueji@ustb.edu.cn or hfdong@ustb.edu.cn

Abstract:

Imaging microRNA (miRNA) in living cells significantly contributes to the research of miRNA-associated physiological and pathological process. The enzyme-free strand displacement cascade amplification (SDCA) strategy provides intriguing prospective for intracellular nucleic acid detection, but the requirement of external catalytic fuel limits its detection sensitivity. Herein, we first design a smart autonomous ATP self-powered SDCA system for high-sensitive multiple intracellular miRNAs detection. Rational engineered Y-motif DNA structures are functionalized on mesoporous silica ($mSiO_2$ NPs)-coated copper sulfide (CuS) nanoparticles loaded with numerous ATP (CuS@$mSiO_2$-Y/ATP) through a pH stimulus-responsive disulfide bond. The SDCA process is implemented by endogenous specific miRNA as trigger and ATP as fuel that mainly released from nanocarrier by pH and photothermal stimulus-responsive. The ATP self-powered SDCA process presents much higher sensitivity enhancement compared to that without amplification for intracellular low-abundance miRNA imaging among different cell lines. Two-color simultaneously and sensitively imaging multiple cancer-related miRNAs in living cells is also confirmed. It enables facile and accurate differentiation between the normal cells by the sensitive intracellular miRNA imaging, which improves the veracity and timeliness for early cancer diagnosis and treatment.

Keywords:

ATP Fuel, Strand-Displacement Cascade Amplification, Intracellular miRNA Detection, pH Stimulus-response

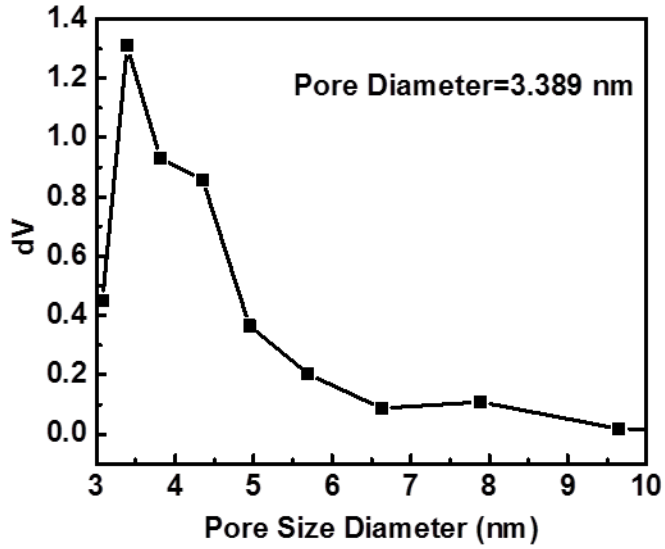

Figure S1. Pore size distribution of CuS@mSiO$_2$-SH NPs.

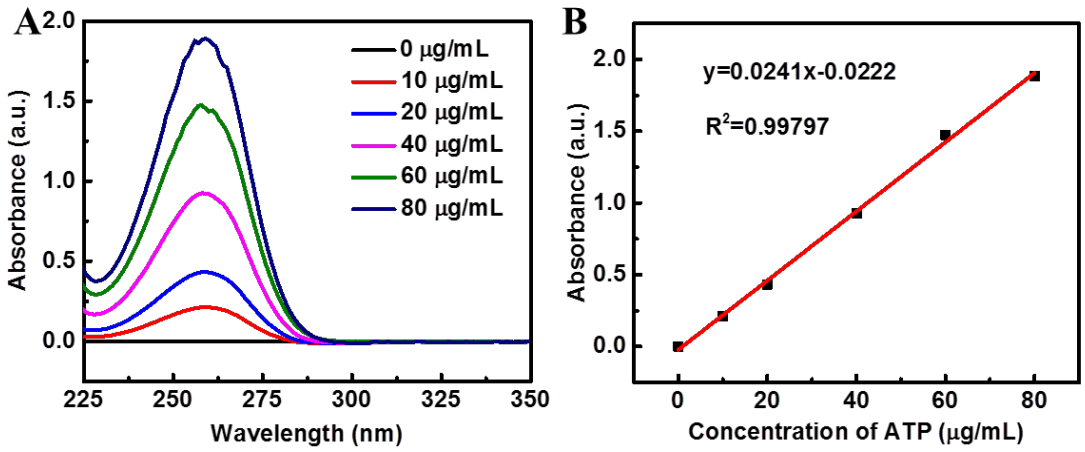

Figure S2. (A) UV-vis absorption spectra of free ATP dispersed in PBS (10 mM, pH 7.4) with different concentration (0-80 μg/mL). (B) Calibration curve between the UV-vis absorbance at 258 nm and the concentration of ATP.

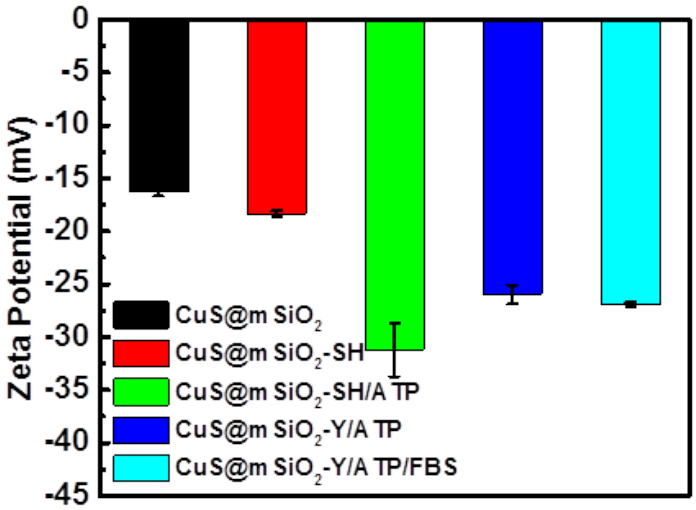

Figure S3. Zeta potential of CuS@mSiO$_2$, CuS@mSiO$_2$-SH, CuS@mSiO$_2$-SH/ATP, CuS@mSiO$_2$-Y/ATP, and CuS@mSiO$_2$-Y/ATP in FBS.

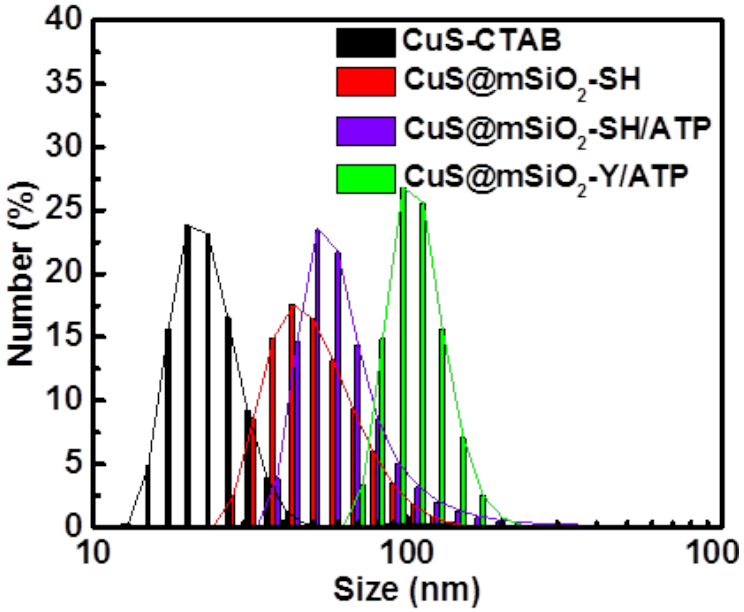

Figure S4. DLS of CuS@mSiO$_2$-CTAB, CuS@mSiO$_2$-SH, CuS@mSiO$_2$-SH/ATP and CuS@mSiO$_2$-Y/ATP.

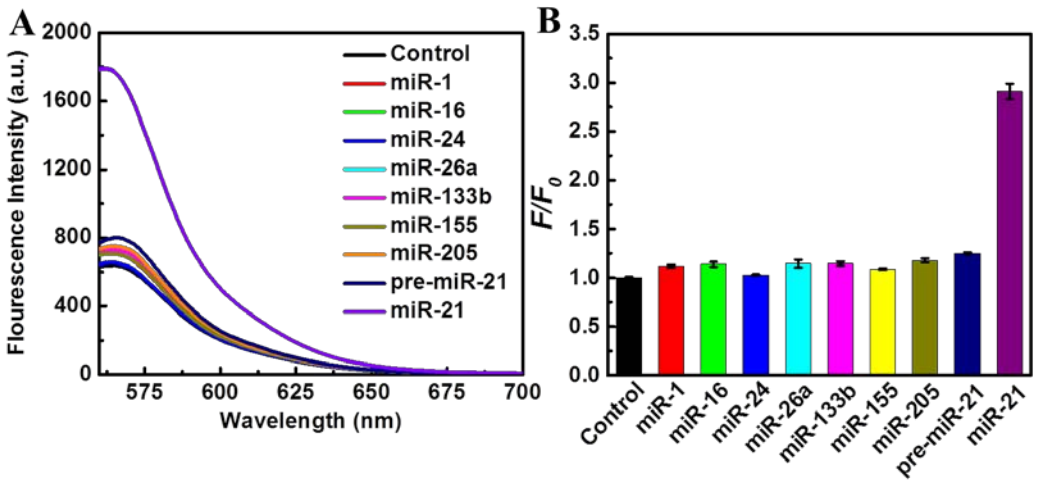

Figure S5. Selectivity of CuS@mSiO$_2$-Y/ATP over several miRNA targets. Error bars were estimated from three replicate measurements.

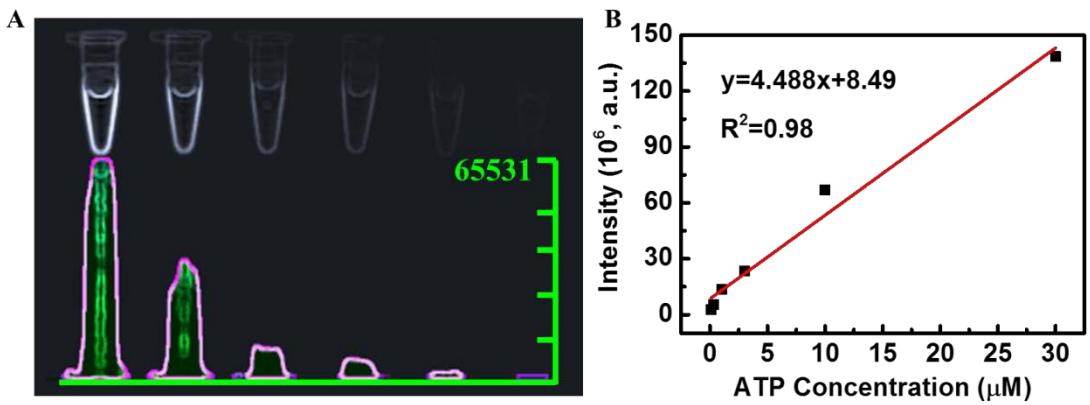

Figure S6. (A) The images of chemiluminiscence and fluorescence intensity for ATP standard solution with different concentration (left to right: 30, 10, 3, 1, 0.3 and 0.1 μM). (B) Calibration curve between the chemiluminiscence intensity and the concentration of ATP standard solution.

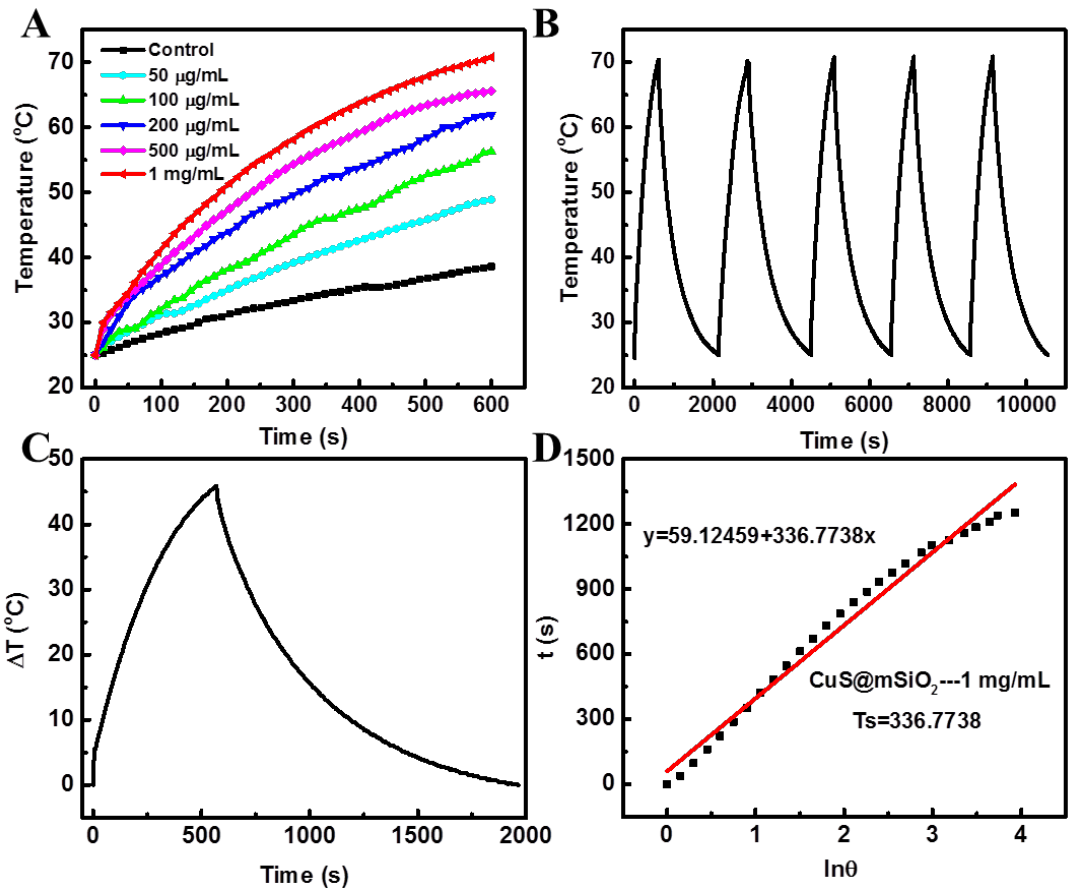

Figure S7. Evaluation of photothermal conversion and stability of CuS@mSiO$_2$-SH NPs. (A) Temperature elevation of CuS@mSiO$_2$-SH NPs dispersed in 1 mL of PBS solution (10 mM, pH 7.4) over a period of 10 min under NIR-laser irradiation (980 nm, 0.7 W/cm^2) at various concentrations from 50 μg/mL to 1 mg/mL, PBS solution as a control. (B) Temperature elevation of CuS@mSiO$_2$-SH NPs dispersed in 1 mL of PBS solution (1 mg/mL) over five NIR-laser on/off cycles under NIR-laser irradiation. (C) One single NIR-laser on (10 min)/off (naturally cooling to room temperature, 25°C) cycle of CuS@mSiO$_2$-SH NPs under NIR-laser irradiation. (D) Cooling period *vs* negative natural logarithm of driving force temperature for calculating the photothermal conversion efficiency. The photothermal conversion efficiency (η value) of CuS@mSiO$_2$-SH NPs is calculated according to the previous report.

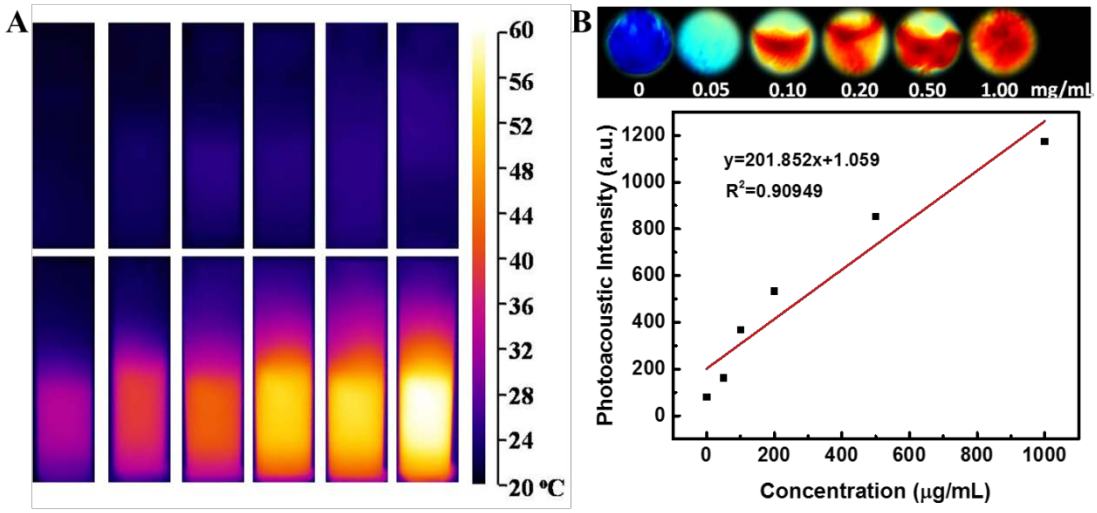

Figure S8. Infra-red (IR) thermal imaging (A) and photoacoustic imaging (B) of CuS@mSiO2-SH NPs aqueous solutions with different concentrations (from 50 μg/mL to 1 mg/mL).

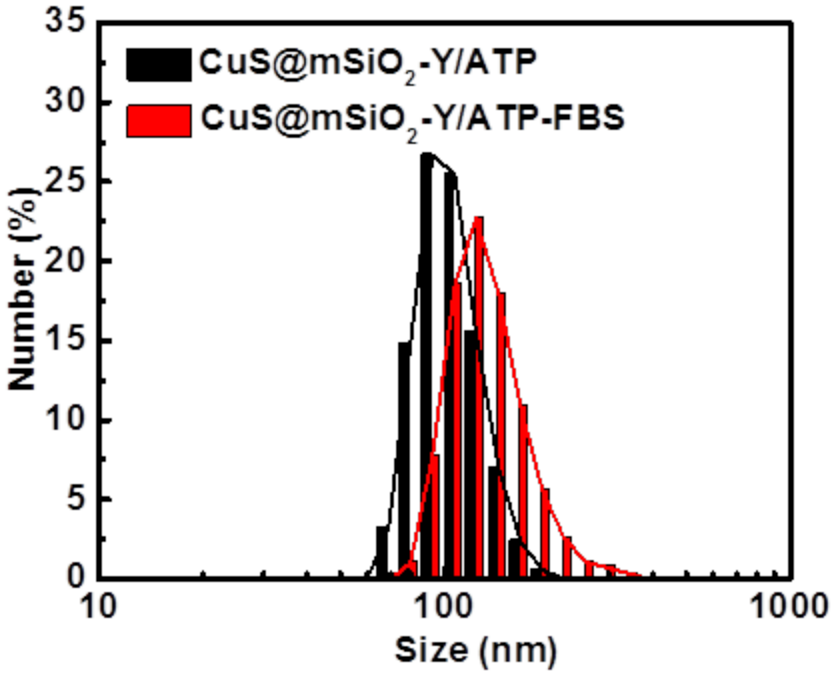

Figure S9. DLS of CuS@mSiO$_2$-Y/ATP in PBS and in FBS, respectively.

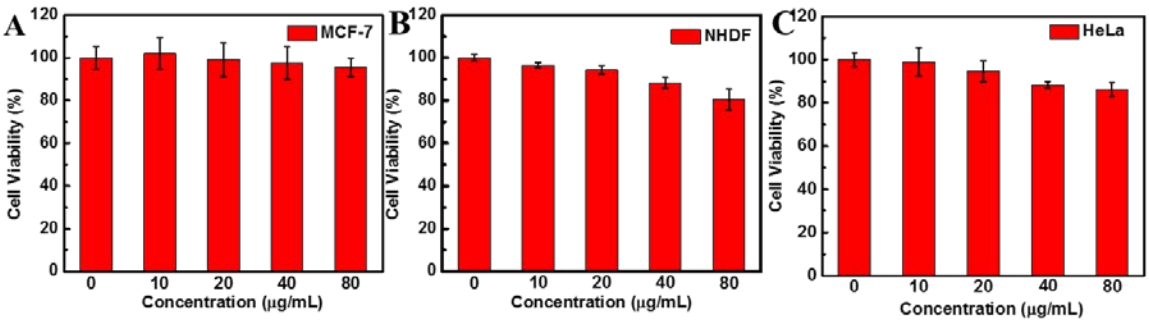

Figure S10. In vitro cytotoxicity of different cells (MCF-7, NHDF and HeLa) were incubated with different concentration of CuS@mSiO$_2$-SH (0-80 μg/mL) in Opti-MEM reduced serum medium. MCF-7 cells (A), NHDF cells (B) and HeLa cells (C) were exposed to CuS@mSiO$_2$-SH NPs.